



## Favorable effects of titanium nitride or its thermally treated version in a gel electrolyte for a quasi-solid-state dye-sensitized solar cell

Chuan-Pei Lee<sup>a</sup>, Lu-Yin Lin<sup>a</sup>, R. Vittal<sup>a</sup>, Kuo-Chuan Ho<sup>a,b,\*</sup>

<sup>a</sup> Department of Chemical Engineering, National Taiwan University, Taipei 10617, Taiwan

<sup>b</sup> Institute of Polymer Science and Engineering, National Taiwan University, Taipei 10617, Taiwan

### ARTICLE INFO

#### Article history:

Received 5 June 2010

Accepted 17 August 2010

Available online 21 August 2010

#### Keywords:

At-rest stability

Dye-sensitized solar cell

Electrochemical impedance spectroscopy

Polymer gel electrolyte

Thermally treated titanium nitride

### ABSTRACT

Titanium nitride (TiN) or its thermally treated version is incorporated into the gel electrolyte of a dye-sensitized solar cell (DSSC) and the consequent effects are investigated in terms of photovoltaic performance of the cell. The gel electrolyte is essentially prepared by using poly(vinylidene fluoride-co-hexafluoropropylene) (PVDF-HFP). With an addition of 3 wt% TiN, the solar-to-electricity conversion efficiency ( $\eta$ ) of the DSSC reaches 5.33% from 4.15% of the cell without TiN. X-ray diffraction (XRD) spectra of thermally treated-TiN (tt-TiN) clearly shows the partial conversion of TiN into TiO<sub>2</sub> with both anatase and rutile crystal phases. The DSSC with the incorporation of 3 wt% of tt-TiN into its electrolyte shows a further improved efficiency of 5.68%, with reference to the efficiency of TiN-incorporated DSSC. The cell with 3 wt% of tt-TiN also shows unflinching at-rest stability after more than 1000 h. Electrochemical impedance spectroscopy (EIS) is used to obtain charge transfer properties of the cells. Crystallinity and crystalline phases are analyzed by X-ray diffraction (XRD) spectra. Surface morphologies are observed with scanning electron microscopy (SEM). IPCE curves substantiate the variations in short circuit photocurrents.

© 2010 Elsevier B.V. All rights reserved.

### 1. Introduction

The solar-to-electricity conversion efficiency ( $\eta$ ) of a quasi-solid-state dye-sensitized solar cell (QSS-DSSC) is presently lesser than that of a liquid electrolyte cell, because a quasi-solid electrolyte is viscous and cannot permeate easily into the pores of the TiO<sub>2</sub> film of the DSSC. Ionic mobility is usually retarded in a polymer gel electrolyte (PGE) owing to the polymer matrix and owing to the viscous nature of the electrolyte, and this is one of the reasons for the reduced performance of a QSS-DSSC, with reference to that of a liquid electrolyte DSSC.

PGEs are considered to be most prospective substitutes for liquid electrolytes in order to fabricate practically applicable QSS-DSSCs, due to their merits such as high ionic conductivity, good interfacial filling property, long-term stability, and above all non-propensity to leakage. The polymers commonly used for PGE systems are: poly(ethylene oxide) (PEO), poly(acrylonitrile) (PAN), poly(methyl methacrylate) (PMMA), poly(vinylidene fluoride) (PVDF), poly(1-vinyl pyrrolidone) (PVP), poly(N-methyl acrylamide) (PDMAA), and poly(1-vinyl pyrrolidone-co-vinyl acetate) (P(VP-C-VA)) [1–6]. Poly(vinylidene fluoride-co-hexafluoropropylene) (PVDF-HFP) copolymer is well-known for its good mechanical stability

and for its feasibility to form a film; it is also known to be a good supporter of liquid electrolyte in terms of the latter's ionic conductivity [7]. Thus, PVDF-HFP copolymer is a viable PGE for an electrochemical photovoltaic device.

Nanomaterials were incorporated as fillers into PGEs to enhance both the cell efficiency and the long-term stability of DSSCs; the nanomaterials include TiO<sub>2</sub>, SiO<sub>2</sub>, graphite nanoparticles, and nanosilicate platelets [2,5,8–11]. Various effects were reported for the incorporation of nanomaterials into a PGE, including reduction of crystallinity of the polymer, formation of transfer channels for the redox couple, and enhancement of thermal stability of the pertinent QSS-DSSC.

Titanium nitride (TiN) is an extremely hard, conducting ceramic material, often used as a coating for metal components to improve their surface properties [12–18]. TiN possesses very good conductivity [19] and it is biocompatible as well [20]. However, the literature on the use of TiN has been limited to its use in supercapacitors [21], as a substrate for electrodeposition of metals such as Pt, Cu, Ag or Zn [22–24], for deactivation of marine bacteria [25], and for electroanalysis [26,27]. Moreover, it was also reported that platinumized TiN is a very good catalyst for the electrochemical oxidation of methanol [28].

By considering these features of TiN, we have used this material as a filler in the PVDF-HFP gelled electrolyte and studied its influence on the performance of the pertinent DSSC. Besides, we studied the effects of thermally treated TiN (tt-TiN) in the PVDF-HFP gelled electrolyte on the photovoltaics of the pertinent DSSCs. The effects

\* Corresponding author at: Department of Chemical Engineering, National Taiwan University, Taipei 10617, Taiwan. Tel.: +886 2 2366 0739; fax: +886 2 2362 3040.  
E-mail address: [kcho@ntu.edu.tw](mailto:kcho@ntu.edu.tw) (K.-C. Ho).

of  $I_2$  concentration on the photovoltaic properties of the cells were also studied to optimize its concentration for the cells. To the best of our knowledge, this is the first report on QSS-DSSCs using TiN or thermally treated TiN in their electrolytes. In addition, at-rest stability of the DSSC with tt-TiN was investigated for more than 1000 h, and compared with that of a cell with a common organic liquid electrolyte.

## 2. Experimental

Lithium iodide (LiI, synthetic grade), iodine ( $I_2$ , synthetic grade), poly(ethylene glycol) (PEG, M.W. = 20,000), and 1-methyl-3-propyl imidazolium iodide (PMII) were obtained from Merk; 4-tert-butylpyridine (TBP, 96%) and tert-butyl alcohol (tBA, 96%) were obtained from Acros; Ti (IV) tetraisopropoxide (TTIP, >98%), acetonitrile (ACN, 99.99%), acetylacetone (AA, >99.5%), ethanol (99.5%), isopropyl alcohol (IPA, 99.5%), and poly(vinylidene fluoride-co-hexafluoropropylene) (PVDH-HFP) were obtained from Aldrich.

Various amounts of titanium nitride (TiN, Wako, 50 nm-sized) were added to the polymer gel electrolyte, composed of 5 wt% PVDH-HFP, 0.1 M LiI, 0.6 M PMII, 0.5 M TBP and an amount of  $I_2$  in 3-methoxypropionitrile (MPN, Fluka), to study the effects of TiN on the performance of the DSSC. As the organic liquid electrolyte, a mixture of the same as above without PVDF-HFP was used. Thermally treated TiN (tt-TiN) nanoparticles were obtained by placing the TiN in an oven at 500 °C for 30 min.

Commercial titanium dioxide (ST-21, 50 m<sup>2</sup> g<sup>-1</sup>, 6 g, Ya Chung Industrial Co. Ltd., Taiwan) was thoroughly mixed in a solution of AA (500  $\mu$ l) in DI-water (11 g). This solution was stirred for 3 days and 1.8 g of PEG was added to this well-dispersed colloidal solution. The final mixture was stirred for further 2 days, and the TiO<sub>2</sub> paste was prepared.

A fluorine-doped SnO<sub>2</sub> conducting glass (FTO, 15  $\Omega$  sq.<sup>-1</sup>, Solaronix S.A., Aubonne, Switzerland) was first cleaned with a neutral cleaner, and then washed with DI-water, acetone, and IPA, sequentially. The conducting surface of the FTO was treated with a solution of TTIP (0.028 g) in ethanol (10 ml) for obtaining a good mechanical contact between the conducting glass and TiO<sub>2</sub> film, as well as to isolate the conducting glass surface from the electrolyte. Thickness of the TiO<sub>2</sub> film was determined using a surface profilometer (Sloan Dektak 3030). From the TiO<sub>2</sub> paste a 10  $\mu$ m-thick film of TiO<sub>2</sub> was coated onto the treated conducting glass by using the doctor blade technique; a portion of 0.4 cm  $\times$  0.4 cm was selected as the active area by removing the side portions by scrapping. The TiO<sub>2</sub> film was gradually heated to 450 °C in an oxygen atmosphere, and subsequently sintered at that temperature for 30 min. After sintering at 450 °C and cooling to 80 °C, the TiO<sub>2</sub> electrode was immersed in a 3  $\times$  10<sup>-4</sup> M solution of N719 (Solaronix S.A., Aubonne, Switzerland) in ACN and tBA (volume ratio of 1:1), at room temperature for 24 h. After dye-adsorption, a 25  $\mu$ m-thick Surlyn<sup>®</sup> (SX1170-25, Solaronix S.A., Aubonne, Switzerland) was put on the dye-sensitized TiO<sub>2</sub> electrode, and the electrode was assembled with a platinum-sputtered conducting glass electrode (ITO, 10  $\Omega$  sq.<sup>-1</sup>). The two electrodes were sealed together by heating. The PVDF-HFP based PGE was heated to 90 °C and then injected into the gap between the electrodes by capillarity. The injecting process was carried out at 90 °C, because the viscosity of PVDF-HFP based PGE was too high for penetration into the gap and needed heating. The electrolyte-injecting hole was made with a drilling machine, and the hole was sealed simultaneously by Surlyn<sup>®</sup> and UV glue (Optocast 3410 40K GEN2, Alexander Jewels Co., Ltd.).

Surface of the DSSC was illuminated by a class-A quality solar simulator (PEC-L11, AM1.5G, Peccell Technologies Inc.). Incident light intensity (100 mW cm<sup>-2</sup>) was calibrated with a standard Si Cell (PECSI01, Peccell Technologies Inc.). Photocurrent–voltage

curves of the DSSCs were obtained with a potentiostat/galvanostat (PGSTAT 30, Autolab, Eco-Chemie, The Netherlands). Crystal phase and crystallinity were analyzed by X-ray diffraction (XRD, MO3XHF, MAC). Morphologies of the PVDF-HFP gelled electrolyte containing TiN or tt-TiN were observed in scanning electron microscopic images (SEM, NanoSEM 230, Nova<sup>TM</sup>). Electrochemical impedance spectra (EIS) were obtained by the above-mentioned potentiostat/galvanostat, equipped with an FRA2 module, under a constant light illumination of 100 mW cm<sup>-2</sup>. The frequency range explored was 10 mHz to 65 kHz. The applied bias voltage was set at the open-circuit voltage of the DSSC, between the counter electrode and the FTO-TiO<sub>2</sub>-dye working electrode, starting from the short-circuit condition; the corresponding ac amplitude was 10 mV. The impedance spectra were analyzed using an equivalent circuit model [29,30]. The ionic conductivity ( $\sigma_S$ ) of the electrolyte could be determined using the following formula:

$$\sigma_S = \frac{dS}{A_S \times R_S} \quad (1)$$

In this equation, the ohmic serial resistance ( $R_S$ ), was determined from Nyquist plot obtained by impedance measurement at room temperature; a device with two platinum electrodes and a 25  $\mu$ m thick spacer with a 5.5 mm hole was used for this purpose. The device constant ( $d_S/A_S$ ) was calculated from a standard cell calibration based on a NaCl solution of 12.9 mS cm<sup>-1</sup> (Model 011006, Thermo Orion). Incident photo-to-current conversion efficiency (IPCE) curves were obtained at short-circuit condition. The light source was a 450 W Xe lamp (Oriol Instrument, model 6266) equipped with a water-based IR filter (Oriol Instrument, model 6123NS); light was focused through a monochromator (Oriol Instrument, model 74100) onto the photovoltaic cell. The monochromator was incremented through the visible spectrum to generate the IPCE ( $\lambda$ ) as defined below

$$\text{IPCE}(\lambda) = 1240 \left( \frac{J_{SC}}{\lambda \phi} \right) \quad (2)$$

where  $\lambda$  is the wavelength,  $J_{SC}$  is short-circuit photocurrent (mA cm<sup>-2</sup>) recorded with a potentiostat/galvanostat, and  $\phi$  is the incident radiative flux (W m<sup>-2</sup>) measured with an optical detector (Oriol Instrument, model 71580) and power meter (Oriol Instrument, model 70310).

## 3. Results and discussion

It is well-known that an efficient transport of iodide and triiodide in the electrolyte is necessary for good performance of a conventional DSSC. Efficient transport of iodide is necessary, because the oxidized dye (dye<sup>+</sup>) should be regenerated by it quickly after the excited dye injects electrons into the conduction band of TiO<sub>2</sub> under illumination. Efficient transport of triiodide is necessary, because in absence of a rapid electron transfer from the counter electrode to triiodide the electrons accumulated at the electrode by the external circuit will lead to a concentration overpotential and to a loss of energy of the DSSC. In view of this, different concentrations of  $I_2$  are used in the PVDF-HFP electrolyte to optimize the concentration for obtaining the best possible photocurrent–voltage ( $I$ – $V$ ) characteristics for the type of DSSCs under investigation. Fig. 1 shows the current–voltage ( $I$ – $V$ ) characteristics of DSSCs, each with a particular concentration of  $I_2$  (M) in its PGE; the measurements were performed both at 100 mW cm<sup>-2</sup> light intensity and in the dark, and the corresponding parameters are listed in Table 1. Conductivity values in Table 1 show that increased amount of  $I_2$  up to 0.2 M results in improved conductivity of the electrolyte, i.e. in an improvement in the ionic mobility in the electrolyte, which occurs in the microscopic molecular networks of the polymer. Such a substantial increase in the conductivity at higher concentrations

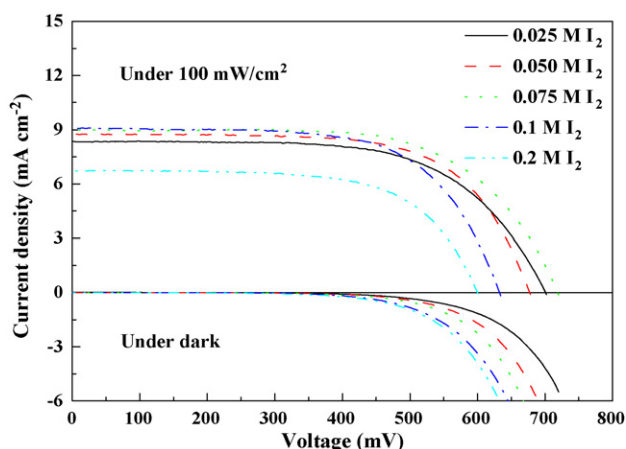
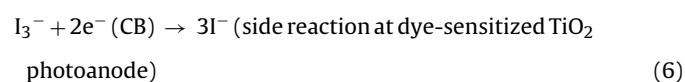


**Fig. 1.** Current–voltage curves of the DSSCs with PGE containing various amounts of  $I_2$  (M), measured at  $100 \text{ mW cm}^{-2}$  light intensity and in the dark.

of  $I_2$  (0.1 M, 0.2 M) may be rationalized on the basis of formation of polyiodides ( $I_{2n+1}^-$ ) in the electrolyte, as reported by Yanagida and co-workers, using Raman spectroscopic analysis [31]. They suggested a Grotthuss-type charge-transfer mechanism, where electron hopping and polyiodides bond exchange were coupled, for the effective conductance of the gel electrolyte, rationalizing the high conductivity of such electrolytes in DSSCs. However, the increased conductivity of the electrolyte with increased concentration of  $I_2$  has not resulted in a matching increase of  $J_{SC}$  for the  $I_2$  concentration of 0.2 M. Those phenomena may be explained by considering the following redox reactions:



According to reaction (3), increase of  $I_2$  concentration acts in favor of  $I_3^-$  as  $I^-$  is much higher than that of  $I_2$ . Since a critical concentration level of  $I_3^-$  is necessary for the cell functioning at the beginning, reactions (4) and (5) proceed effectively and the  $J_{SC}$  increases and saturates at a particular point. Further increase in the concentration of  $I_2$  favors the formation of an excess of  $I_3^-$ , and thereby favors the reaction (6); this facilitates recombination of injected conduction band (CB) electrons with polyiodides, and increases the dark current as shown in Fig. 1. This increase in the dark current decreases the  $V_{OC}$  of the cell. Furthermore, increasing content of  $I_2$  leads to enhanced light absorption even in the visible range by the carrier mediators, which exist in the porous dye-

**Table 1**

Photovoltaic parameters of the DSSCs with PGE containing various amounts of  $I_2$  (M). The table also shows conductivity of the electrolyte with different concentrations of  $I_2$ .

$I_2$ (M)	$V_{OC}$ (mV)	$J_{SC}$ ( $\text{mA cm}^{-2}$ )	FF	$\eta$ (%)	$\sigma_s^a$ ( $\text{mS cm}^{-1}$ )
0.025	700	8.36	0.63	3.68	8.15
0.05	676	8.77	0.66	3.92	8.43
0.075	718	8.94	0.64	4.15	8.66
0.1	633	9.09	0.65	3.71	9.22
0.2	599	6.74	0.65	2.62	9.58

<sup>a</sup> Conductivities ( $\sigma_s$ ) were determined through electrochemical impedance measurements at room temperature; a device with two platinum electrodes and a  $25 \mu\text{m}$ -thick spacer with a 5.5 mm hole was used.

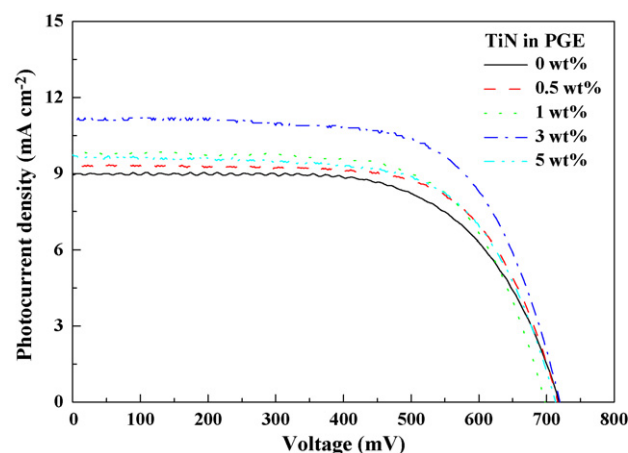


**Fig. 2.** Photocurrent–voltage curves of the DSSCs with PGE containing various amounts of TiN (wt%), measured at  $100 \text{ mW cm}^{-2}$  light intensity.

adsorbed  $\text{TiO}_2$  matrix. This enhanced light absorption decreases the light-harvesting capacity of the dye molecules [32] and thereby decreases the corresponding  $J_{SC}$ . Thus, not only the  $V_{OC}$  but also the  $J_{SC}$  decreased for the cell with 0.2 M  $I_2$ . As can be seen in Table 1, the optimal cell efficiency of 4.15% is obtained for the PVDF-HFP based DSSC with 0.075 M of  $I_2$ ; the cell shows a fill-factor (FF) of 0.64, an open-circuit voltage ( $V_{OC}$ ) of 718 mV, and a short-circuit current density ( $J_{SC}$ ) of  $8.94 \text{ mA cm}^{-2}$ . Accordingly, we have performed further experiments with a concentration of 0.075 M of  $I_2$ .

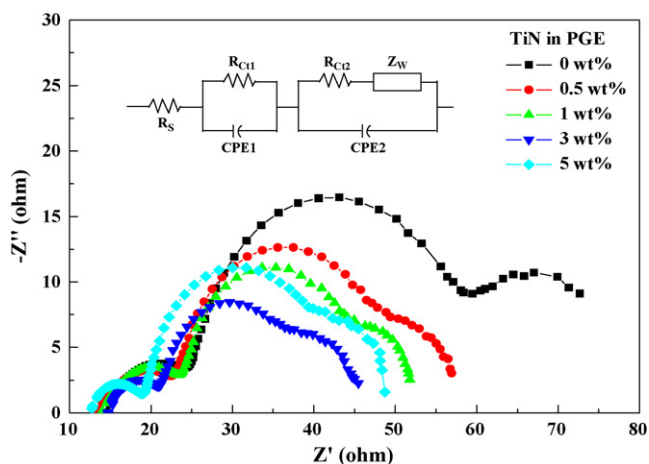
Incorporation of nano-filler into PGE was reported to enhance the performance of a DSSC [2,5,8–11], circumventing the sealing problem, and increase the stability of the device. Meanwhile, TiN was considered to be a unique conducting ceramic material, due to its high conductivity and thermal-stability [12–28]. Therefore, we incorporated this conducting ceramic material as an alternative filler into the PVDF-HFP based PGE.

Fig. 2 shows the photocurrent–voltage curves of DSSCs with PVDF-HFP based PGE containing various amounts of TiN (wt%). The corresponding open-circuit potential ( $V_{OC}$ ), short-circuit current ( $J_{SC}$ ), fill factor (FF) and cell efficiency ( $\eta$ ) are listed in Table 2. It is noted that the cell efficiency increases with the increase of TiN nanoparticles from 0.5 wt% to 3 wt%, and further increase of TiN decreases the cell efficiency. Nano-TiN contents of 0.5 wt%, 1 wt%, and 3 wt% could enhance the ionic conductivity of PGE owing to the decrease in the crystallinity of PVDF-HFP matrix; at this levels of TiN it acts as “solid plasticizer” to improve the ion-transport property of the PGE. Li et al. [33] have studied the electrochemical properties and changes in crystallinity of PVDF-HFP, filled with different amounts of  $\text{Al}_2\text{O}_3$  nanoparticles. They found that the crystallinity of this polymer matrix decreased with the increase of mass fraction of nanoparticles, due to their solid plasticization effect. Recently, Kang et al. [34] studied QSS-DSSCs, employing ternary component PGEs, and suggested that  $\text{TiO}_2$  nanoparticles added to a PGE as nanofiller can decrease the crystallinity of the polymer and build transfer channels for the redox couple, and thereby cause a

**Table 2**

Photovoltaic parameters of the DSSCs with PGE containing various amounts of TiN (wt%). The table also shows electrochemical impedance spectroscopic parameters, namely  $R_{ct1}$ ,  $R_{ct2}$ , and  $R_{diff}$ .

TiN (wt%)	$V_{OC}$ (mV)	$J_{SC}$ ( $\text{mA cm}^{-2}$ )	FF	$\eta$ (%)	$R_{ct1}$	$R_{ct2}$	$R_{diff}$
0	718	8.94	0.64	4.15	14.11	39.53	31.33
0.5	716	9.29	0.67	4.49	11.83	28.89	22.17
1	696	9.81	0.67	4.58	12.71	26.10	15.52
3	718	11.09	0.67	5.33	7.50	21.52	13.71
5	714	9.75	0.65	4.55	7.12	27.48	23.31



**Fig. 3.** Electrochemical impedance spectra of the DSSCs with PGE containing various amounts of TiN (wt%), measured at  $100 \text{ mW cm}^{-2}$  light intensity under the open-circuit voltage. The inset shows the equivalent circuit.

significant increase in the  $J_{SC}$  for the corresponding DSSC. Excessive addition of TiN nanoparticles, e.g. 5 wt% of it, can increase the viscosity of the electrolyte and decrease the motion of  $I^-$  and  $I_3^-$  in it; this decrease in ion motion leads to a decrease in  $J_{SC}$  and FF, because ionic conductivity of an electrolyte directly effects FF. The slightly decreased  $V_{OC}$  in the case of 5 wt% of TiN, with reference to that of 3 wt% of TiN is in accordance to their  $J_{SC}$  values, because deficient dye-regeneration due to slow  $I^-$  motion favors increased recombination reactions between the conduction band electrons and  $I_3^-$  ions and thereby a decrease in  $V_{OC}$ . The cell in the case of 5 wt% of TiN with decreased  $J_{SC}$ , FF, and  $V_{OC}$  thus showed a reduced efficiency compared to that of the cell with 3 wt% of TiN which thus proved to be the optimum level of TiN for the type of cells studied here.

For further study, electrochemical impedance spectroscopy (EIS) technique was employed to analyze the interfacial resistances in the DSSCs. Fig. 3 shows the electrochemical impedance spectra of the DSSCs with the configuration FTO/TiO<sub>2</sub>/dye/PGE/Pt/ITO containing different weight percentages of TiN in the PGE. The equivalent circuit is shown as the inset of the figure. In general, EIS spectrum of a DSSC shows three semicircles in the frequency range of 10 mHz to 65 kHz. The ohmic serial resistance ( $R_S$ ) corresponds to the overall series resistance. The first and second semicircles are assigned to the charge-transfer resistances at the counter electrode ( $R_{ct1}$ ) and the TiO<sub>2</sub>/dye/PGE interface ( $R_{ct2}$ ), respectively. The Warburg diffusion process of  $I^-/I_3^-$  in the electrolyte ( $R_{diff}$ ) is the third semicircle. Electrochemical impedance spectroscopic parameters are shown in Table 2. It can be seen in Table 1 that both  $R_{diff}$  and  $R_{ct2}$  decrease for TiN contents up to 5 wt%, compared to those without TiN. Presumably, the self-aggregation of the polymer was retarded due to the incorporation of TiN into the polymer gel electrolyte (PGE); this retarded self-aggregation of the polymer is favorable for diffusion of  $I^-/I_3^-$  ions in the electrolyte as can be seen by the decrease  $R_{diff}$  for all the additions, with reference to the  $R_{diff}$  for the bare electrolyte. Increased diffusion of  $I^-$  ions in the electrolyte leads to decreased charge transfer resistance at TiO<sub>2</sub>/dye/PGE interface, as can be seen with decreased  $R_{ct2}$  for all the cases of electrolytes with TiN, compared to the case of bare electrolyte. These decreased  $R_{diff}$  and  $R_{ct2}$  for the cells with TiN are in consistency with the corresponding increases in  $J_{SC}$ 's of the cells, compared to that of the cell without any TiN.

Out of curiosity, we tried to replace the TiN in the electrolyte with a thermally treated TiN (tt-TiN). In the XRD pattern in Fig. 4(a), the tt-TiN shows clear peaks corresponding to (101) and (110) of TiO<sub>2</sub>, namely, the anatase and rutile crystal phases, respectively; the peaks corresponding to (111) and (200) of TiN structure still

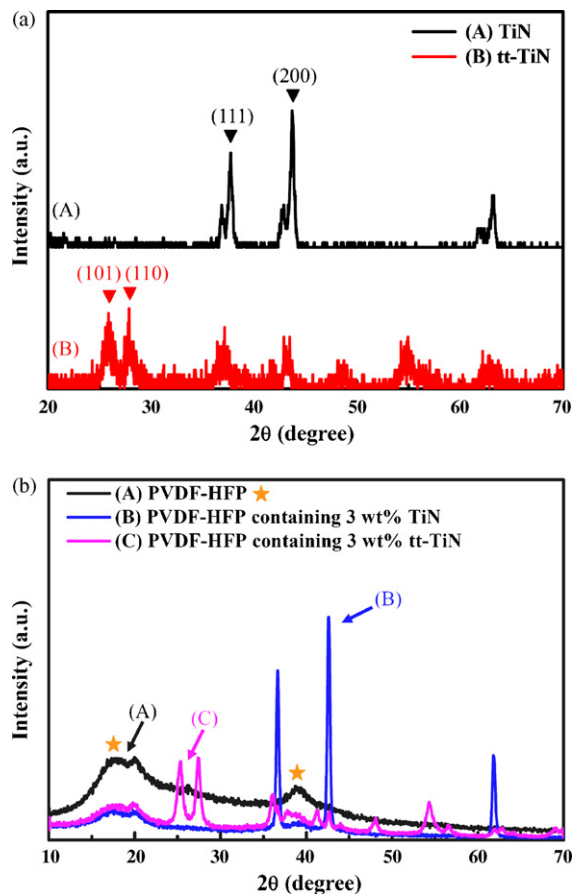


**Fig. 4.** (a) X-ray diffraction patterns of TiN before and after sintering at 500 °C; (b) X-ray diffraction patterns of the PVDF-HFP polymer film without or with the addition of 3 wt% TiN or 3 wt% tt-TiN.

continue to exist in the XRD pattern of tt-TiN, but with decreased intensity, with reference to those obtained for TiN before its thermal treatment. Thus, the XRD pattern in Fig. 4(a) confirms the partial formation of TiO<sub>2</sub> from TiN.

The retardation of self-aggregation of the polymer due to the incorporation of TiN is confirmed through XRD analysis and SEM images. A comparison among the XRD patterns of PVDF-HFP, PVDF-HFP with 3 wt% of TiN and PVDF-HFP with 3 wt% of tt-TiN in Fig. 4(b) shows clearly a decrease in the crystallinity of polymer with the incorporation of TiN or tt-TiN. This decreased crystallinity of the polymer with the incorporation of TiN or tt-TiN is also confirmed through SEM images. Fig. 5(a) shows the SEM image of bare PVDF-HFP, Fig. 5(b) that of the polymer with 3 wt% of TiN, and Fig. 5(c) that of polymer with 3 wt% of tt-TiN. While the bare polymer shows large aggregated grains of it distributed more or less uniformly and with large gaps among them, the polymer with TiN or tt-TiN shows uniform and non-aggregated polymer containing nanoparticles or clusters of nanoparticles of TiN. In other words the polymer with TiN or tt-TiN is relatively amorphous with reference to its bare form.

The relatively amorphous PVDF-HFP with more homogeneous distribution of the polymer molecules due to the addition of TiN or tt-TiN facilitates a better connection between the polymer and the counter electrode [5]. Thus, a reduction of  $R_{ct1}$  was also observed for all TiN additions (Table 2). Table 2 shows that  $R_{diff}$  and  $R_{ct2}$  have increased with 5 wt% of TiN, with reference to those of 3 wt% of TiN; this can be now attributed to the decreased ion motion inside the channels of the polymer with excessive addition of TiN (5 wt%) and the associated poor penetration of the electrolyte into the porous of TiO<sub>2</sub> [2]. These results are in consistency with the corresponding photovoltaic parameters of DSSCs with 3 and 5 wt% of TiN.

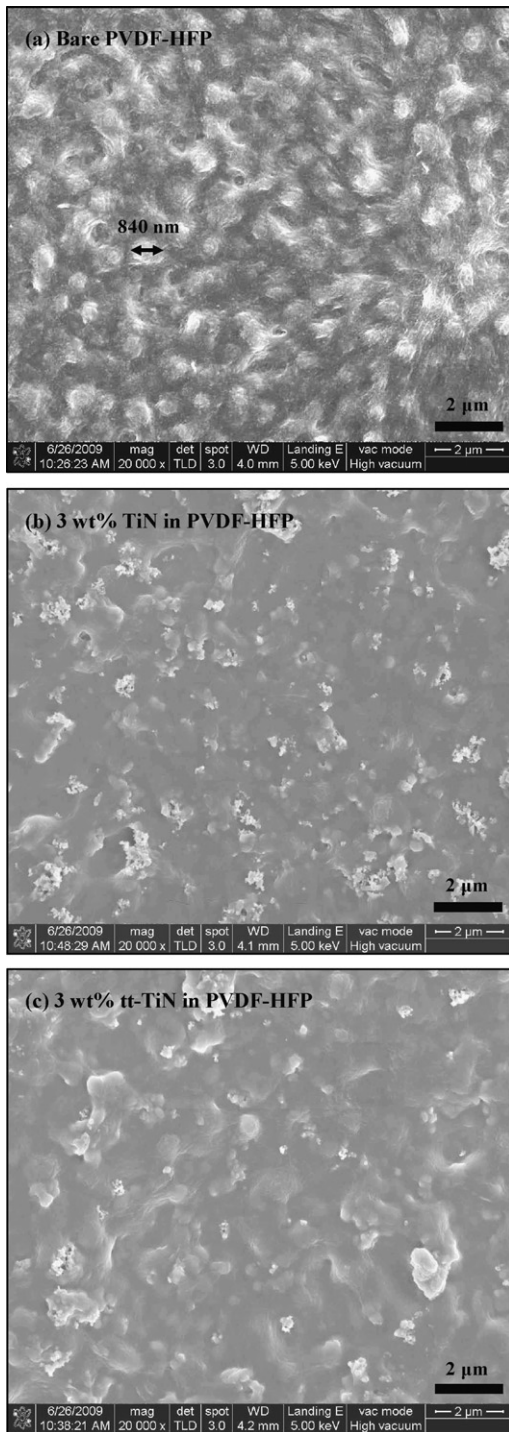


**Fig. 5.** Scanning electron microscopic images of the PVDF-HFP polymer films without or with the addition of 3 wt% TiN or 3 wt% tt-TiN.

As shown in Fig. 6(a), when TiN was replaced with tt-TiN in the polymer electrolyte, the cell efficiency has further increased to 5.68% ( $V_{OC} = 728$  mV,  $J_{SC} = 11.81$  mA cm<sup>-2</sup>, and FF = 0.66), at 3 wt% of TiN. As shown in Fig. 6(b), the interfacial resistances for the DSSCs with 3 wt% TiN and 3 wt% of tt-TiN are almost the same. We suggest that the slight improvement in the efficiency of the DSSC with 3 wt% of tt-TiN, with reference to that of the DSSC with 3 wt% of TiN is due to the light scattering effect by the rutile crystal phase of TiO<sub>2</sub> formed in the case of tt-TiN (Fig. 4(a) and (b)), which is not the case for the cell with TiN. This explanation is also confirmed by IPCE measurements as shown in Fig. 7. Fig. 7 illustrates the IPCE curves

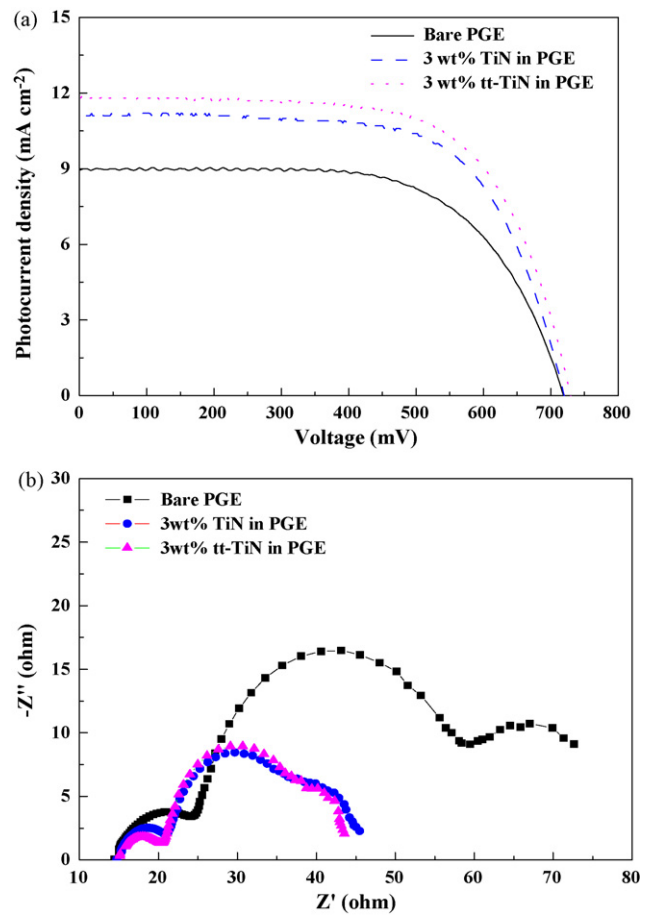


**Fig. 6.** (a) Photocurrent–voltage curves of the DSSCs with bare PGE, PGE containing 3 wt% of TiN, and PGE containing 3 wt% of tt-TiN; (b) corresponding electrochemical impedance spectra.

of DSSCs without and with 3 wt% of TiN or 3 wt% of tt-TiN. The broad IPCE curves, covering almost the entire visible spectrum from 350 to 700 nm exhibit maximum values of about 69% for the cells with TiN and about 50% for the cell without it; these values are in consistency with the higher  $J_{SC}$  values of the cells with TiN (11.09 mA cm<sup>-2</sup>) and with tt-TiN (11.81 mA cm<sup>-2</sup>) than that of the cell without any of them (8.94 mA cm<sup>-2</sup>). The higher IPCE values for the cell with tt-TiN

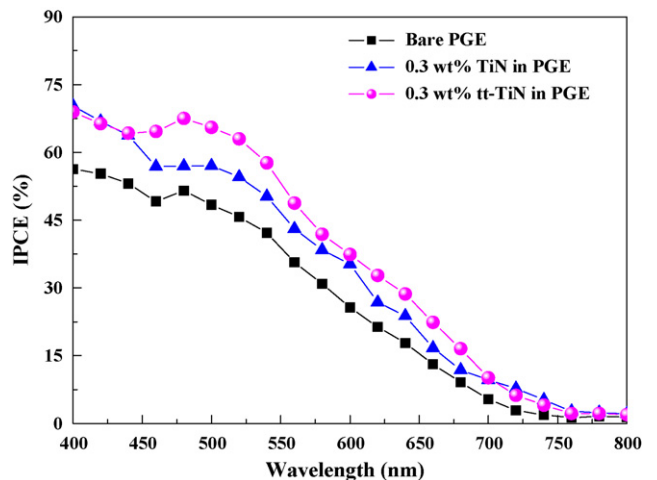


**Fig. 7.** Incident photo-to-current conversion efficiencies (IPCE) of the DSSCs without and with TiN or tt-TiN in the electrolyte.

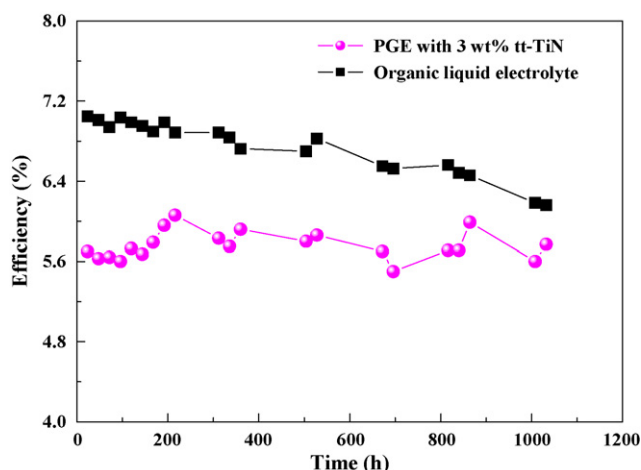


**Fig. 8.** At-rest stability data of the DSSC with PGE containing 3 wt% of tt-TiN and of the DSSC with organic liquid electrolyte.

than those of the cell with TiN is attributed to the light scattering effect in the former case due to its rutile  $\text{TiO}_2$  content. This higher IPCE values rendered a higher  $J_{SC}$  ( $11.81 \text{ mA cm}^{-2}$ ) to the cell with tt-TiN, compared to that of the cell with TiN ( $11.09 \text{ mA cm}^{-2}$ ) and thereby a higher  $\eta$  to the former cell.

As expected, the best DSSC in this study showed an excellent stability and the cell with an organic liquid electrolyte showed instability. Fig. 8 shows at-rest stability of the DSSC with PGE containing 3 wt% of tt-TiN and also that of a cell with organic liquid electrolyte. In this experiment, all cells were sealed by Surlyn® and UV glue, simultaneously. The cell efficiencies were measured everyday in the first week to obtain the average value for the first week, and thereafter every weekend; the cell was stored under dark at room temperature during this test period. Efficiencies were normalized to the average value of first week, because, according to our experience, the cell efficiency reaches a stable value at room temperature in about 7 days. Although the overall power conversion efficiency of the DSSC with organic liquid electrolyte is still higher after more than 1000 h, it has decreased by about 12%. In spite of the fact that the boiling point of the organic solvent, MPN, is  $164^\circ\text{C}$ , its DSSC showed considerable decay in cell performance. On the contrary, the overall power conversion efficiency of the DSSC with tt-TiN has shown an unflinching stability.

#### 4. Conclusions

In summary, for the first time titanium nitride (TiN) and its thermally derived composite (tt-TiN) are proved to enhance the solar-to-electricity conversion efficiency ( $\eta$ ) of a quasi-solid-state DSSC (QSS-DSSC), and the thermally treated TiN (tt-TiN) renders a slightly higher  $\eta$  to its DSSC, with reference to that of the cell with TiN. XRD analysis confirm the partial conversion of TiN into  $\text{TiO}_2$  (anatase and rutile) due to the thermal treatment of the TiN. XRD analysis and SEM images confirm a decrease in the crystallinity of the polymer (PVDF-HFP) electrolyte due to the addition of TiN or tt-TiN. Better performance of the QSS-DSSC with TiN or tt-TiN is proved to be due to the reduced crystallinity of the polymer electrolyte with TiN or tt-TiN, with reference to that of a bare polymer

electrolyte. IPCE values of the DSSCs with bare electrolyte and with electrolytes containing TiN or tt-TiN are consistent with the  $J_{SC}$  values of the corresponding cells. Rutile  $\text{TiO}_2$  content in the tt-TiN renders to its DSSC the best cell efficiency in this study. Finally the QSS-DSSC with 3 wt% of tt-TiN shows an unflinching stability at room temperature for more than 1000 h.

#### Acknowledgements

This work was supported in part by the National Research Council of Taiwan under grant numbers NSC 96-2120-M-002-016, NSC 97-2120-M-002-012 and NSC 98-2120-M-002-003. Some of the instruments used in this study were made available through the financial support of the Academia Sinica, Nankang, Taipei, Taiwan.

#### References

- [1] J. Wu, S. Hao, Z. Lan, J. Lin, M. Huang, Y. Huang, L. Fang, S. Yin, T. Sato, *Adv. Funct. Mater.* 17 (2007) 2645–2652.
- [2] Y. Ying, C.H. Zhou, S. Xu, H. Hu, B.L. Chen, J. Zhang, S.J. Wu, W. Liu, X.Z. Zhao, *J. Power Sources* 185 (2008) 1492–1498.
- [3] K.M. Abraham, M. Alamgir, *J. Electrochem. Soc.* 137 (1990) 1657–1658.
- [4] Z. Jiang, B. Carrol, K.M. Abraham, *Electrochim. Acta* 42 (1997) 2667–2677.
- [5] J. Zhang, Y. Yang, S. Wu, S. Xu, C. Zhou, H. Hu, B. Chen, X. Xiong, B. Sebo, H. Han, X. Zhao, *Nanotechnology* 19 (2008) 245202.
- [6] Z. Lan, J. Wu, S. Hao, J. Lin, M. Huang, Y. Huang, *Energy Environ. Sci.* 2 (2009) 524–528.
- [7] C. Capiglia, Y. Saito, H. Kataoka, T. Kodama, E. Quartarone, P. Mustarelli, *Solid State Ionics* 131 (2000) 291–299.
- [8] T. Stergiopoulos, L.M. Arabatzi, G. Katsaros, P. Falaras, *Nano Lett.* 2 (2002) 1259–1261.
- [9] P. Wang, S.M. Zakeeruddin, M. Grätzel, *J. Fluorine Chem.* 125 (2004) 1241–1245.
- [10] Y.L. Lee, Y.J. Shen, Y.M. Yang, *Nanotechnology* 19 (2008) 455201.
- [11] Y.H. Lai, C.W. Chiu, J.G. Chen, C.C. Wang, J.J. Lin, K.C. Ho, *Sol. Energy Mater. Sol. Cells* 93 (2009) 1860–1864.
- [12] M. Li, S. Luo, C. Zeng, J. Shen, H. Lin, C. Cao, *Corros. Sci.* 46 (2004) 1369–1380.
- [13] Y. Wang, D.O. Northwood, *J. Power Source* 165 (2007) 293–298.
- [14] Y. Wang, D.O. Northwood, *Int. J. Hydrogen Energy* 32 (2007) 895–902.
- [15] A.A.C. Recco, D. López, A.F. Bevilacqua, F. da Silva, A.P. Tschiptschin, *Surf. Coat. Technol.* 202 (2007) 993–997.
- [16] S.T. Myung, M. Kumagai, R. Asaishi, Y.K. Sun, H. Yashiro, *Electrochem. Commun.* 10 (2008) 480–484.
- [17] W. Schintlmeister, O. Pacher, K. Pfaffinger, T. Raine, *J. Electrochem. Soc.* 123 (1976) 924–929.
- [18] J.S. Cho, S.W. Nam, J.S. Chun, *J. Mater. Sci.* 17 (1982) 2495–2502.
- [19] M. Wittmer, B. Studer, H. Melchior, *J. Appl. Phys.* 52 (1981) 5722–5726.
- [20] T. Röstlund, P. Thomsen, L.M. Bjursten, L.E. Ericson, *J. Biomed. Mater. Res.* 24 (1990) 847–860.
- [21] D. Choi, P.N. Kumta, *J. Electrochem. Soc.* 153 (2006) A2298–A2303.
- [22] H. Cesiulis, M. Ziomek-Moroz, *J. Appl. Electrochem.* 30 (2000) 1261–1268.
- [23] S.A.G. Evans, J.G. Terry, N.O.V. Plank, A.J. Walton, L.M. Keane, C.J. Campbell, P. Ghazal, J.S. Beattie, T.J. Su, J. Crain, A.R. Mount, *Electrochem. Commun.* 7 (2005) 125–129.
- [24] E.E. Ferapontova, J.G. Terry, A.J. Walton, C.P. Mountford, J. Crain, J.A.H. Buck, P. Dickinson, C.J. Campbell, J.S. Beattie, P. Ghazal, P.A.R. Mount, *Electrochem. Commun.* 9 (2007) 303–309.
- [25] T. Nakayama, H. Wake, K. Ozawa, H. Kodama, N. Nakamura, T. Matsunaga, *Environ. Sci. Technol.* 32 (1998) 798–801.
- [26] Y. Wang, H. Yuan, X. Lu, Z. Zhou, D. Xiao, *Electroanalysis* 18 (2006) 1493–1498.
- [27] C.N. Kirchner, K.H. Hallmeier, R. Szargan, T. Raschke, C. Radehaus, G. Wittstock, *Electroanalysis* 19 (2007) 1023–1031.
- [28] O.T.M. Musthafa, S. Sampath, *Chem. Commun.* (2008) 67–69.
- [29] L. Han, N. Koide, Y. Chiba, T. Mitate, *Appl. Phys. Lett.* 84 (2004) 2433–2435.
- [30] L. Han, N. Koide, Y. Chiba, A. Islam, T. Mitate, C. R. Chim. 9 (2006) 645–651.
- [31] W. Kubo, K. Murakoshi, T. Kitamura, S. Yoshida, M. Haruki, K. Hanabusa, H. Shirai, Y. Wada, S. Yanagida, *J. Phys. Chem. B* 105 (2001) 12809–12815.
- [32] H. Wang, X. Liu, Z. Wang, H. Li, D. Li, Q. Meng, L. Chen, *J. Phys. Chem. B* 110 (2006) 5970–5974.
- [33] Z. Li, G. Su, X. Wang, D. Gao, *Solid State Ionics* 176 (2005) 1903–1908.
- [34] M.S. Kang, K.S. Ahn, J.W. Lee, *J. Power Sources* 180 (2008) 896–901.